Progress In Electromagnetics Research, Vol. 139, 247–263, 2013

SCATTERED FIELD COMPUTATION WITH AN EXTENDED FETI-DPEM2 METHOD

Ivan Voznyuk, Hervé Tortel*, and Amélie Litman

Institut Fresnel, Aix-Marseille Université, CNRS, Ecole Centrale Marseille, Campus de St Jérôme, Marseille, Cedex 13397, France

Abstract—Due to the increasing number of applications in engineering design and optimization, more and more attention has been paid to full-wave simulations based on computational electromagnetics. In particular, the finite-element method (FEM) is well suited for problems involving inhomogeneous and arbitrary shaped objects. Unfortunately, solving large-scale electromagnetic problems with FEM may be time consuming. A numerical scheme, called the dual-primal finite element tearing and interconnecting method (FETI-DPEM2), distinguishes itself through the partioning on the computation domain into non-overlapping subdomains where incomplete solutions of the electrical field are evaluated independently. Next, all the subdomains are "glued" together using a modified Robin-type transmission condition along each common internal interface, apart from the corner points where a simple Neumann-type boundary condition is imposed. We propose an extension of the FETI-DPEM2 method where we impose a Robin type boundary conditions at each interface point, even at the corner points. We have implemented this Extended FETI-DPEM2 method in a bidimensional configuration while computing the field scattered by a set of heterogeneous, eventually anistropic, scatterers. The results presented here will assert the efficiency of the proposed method with respect to the classical FETI-DPEM2 method, whatever the mesh partition is arbitrary defined.

1. INTRODUCTION

The finite element method applied to the resolution of time harmonic electromagnetic wave scattering has become very popular over the past decades. Among the different techniques, the resolution of the weak

Received 1 February 2013, Accepted 19 March 2013, Scheduled 27 April 2013

* Corresponding author: Hervé Tortel (herve.tortel@fresnel.fr).

form of the Helmholtz equation has shown its potential and versatility for handling a large range of configurations (complex media, periodic structures, anisotropic media ... [1–8]).

In this method, the unknown of interest (the electric or magnetic field) is expanded onto a set of ad-hoc basis functions, classically P1 Lagrange basis functions in 2D or edge basis functions in 3D. Then, a linear system is defined by projecting the Helmholtz equation onto the same set of test functions, as proposed in the Galerkin method. The efficiency of the method mainly depends on the ability of inverting the associated global sparse linear system. This type of problem is strongly dimension dependent and, if in 2D, the use of direct solvers like [9–12] is obvious (a typical scattering problem with 10^6 unknowns is solved in few dozen of seconds on a classical PC), the resolution of the linear system arising from the discretization of 3D configurations with a direct solver is much more tricky, time and memory consuming.

A lot of efforts have been devoted to the development of iterative methods such as multi-grid methods [13], but the problem is still open (for a review see for example [14]). Among the different schemes proposed in order to solve large scale models and preserve the versatility of the method, one can cite the Domain Decomposition Method (DDM) and its different evolutions [15–18].

Related FETI (Finite Element Tearing and Interconnecting) method also seems very robust when one is dealing with arbitrary mesh partitions. The general principle of FETI methods is first to divide the entire computational domain into non-overlapping subdomains. In each of these subdomains, a direct solver is employed for factorizing the matrix arising from the discretization of the Helmholtz equation with which we are concerned. The different adjacent subdomains are then glued at their common interfaces thanks to Lagrange multipliers. The global interface problem is then solved using an iterative algorithm. Finally the solution of the interface problem serves as the right-hand-side of each local problem. This method has been applied in many domains like mechanics [19, 20], acoustic wave propagation [21–23], and in electromagnetism [24–32]. For example, related DDM methods have been developed for simulating the interactions of photonic crystals with electromagnetic waves [33, 34].

Equipping each interface with two Lagrange multipliers is equivalent to imposing a Robin type boundary condition at the interface between each sub-problem. This avoids the appearing of spurious solutions. This boundary condition can also be seen as a crude approximation of a transparency operator and many efforts have been done for optimizing the coefficients arising in this boundary condition, but only when the interfaces between subdomains are

plane [23, 30, 31, 35].

In addition, in order to further improve the convergence of the iterative process and the scalability of the method, one can notice the existence of two techniques: the first one uses the plane wave spectrum operator [21], the second one uses dual-primal techniques which can be seen as coarse grid corrections [22, 26, 28, 36]. In this last method, the corner nodes in 2D or the corner edges in 3D (we denote by "corner" the geometrical entities which belong to more than two subdomains) are extracted from each subdomain and are globally and uniquely numbered.

In the work presented here, we propose an extension of these dual-primal techniques by enforcing a Robin-type boundary condition (with two Lagrange multipliers) not only on the edges related to the internal interfaces but also to the ones related to the corner nodes. Indeed, in the methods already proposed, only one Lagrange multiplier was applied to these corner nodes, yielding a local Neumann boundary condition.

We will demonstrate in the following that the proposed extension more efficiently simulates the scattering from two-dimensional objects made of either isotropic or anisotropic materials. We have focus our attention so far on two-dimensional configurations as it allows easiest comparisons between different methods.

The paper is organized as follows. Section 2 describes the considered electromagnetic scattering configuration. In particular, a total field formulation and a scattered field formulation are detailed. In Section 3, following the notations used in [28], we present our novel approach and derive the linear system obtained for the various interfaces unknowns, either the corner nodes or the inner interface nodes. In Section 4, we present numerical results obtained for 2D scattering problems with anisotropic materials such as Perfectly Matched Layer (PML) boundary conditions. Comparisons with the results obtained with the already existing FETI-DPEM2 method [28] are displayed. We will also show that our method can handle arbitrary mesh partitions. Conclusions follow.

2. FINITE ELEMENT FORMULATION OF THE ELECTROMAGNETIC PROBLEM

We consider an electromagnetic scattering problem, where a known incident electromagnetic wave is impinging on an inhomogeneous target. The incident field, $\mathbf{E}^{\text{inc}}(\vec{r})$, is the field that would exist in the bounded computational domain, denoted as Ω, when no scatterers exist. We will only consider here a two-dimensional configuration

with a s-polarized field and a time dependency in $\exp(-j\omega t)$. In this framework, the incident field satisfies the following Helmholtz equation

$$\operatorname{div}\left(\frac{1}{\mu_r^{\text{inc}}}\operatorname{grad}\mathbf{E}^{\text{inc}}\right) + k_0^2\varepsilon_r^{\text{inc}}\mathbf{E}^{\text{inc}} = -jk_0Z_0\mathbf{J},\ \text{in}\ \Omega \tag{1}$$

where k_0 corresponds to the vacuum wave-number and Z_0 to its intrinsic impedance, $\mu_r^{\text{inc}} = \mu_r^{\text{inc}}(\vec{r})$ (resp. $\varepsilon_r^{\text{inc}} = \varepsilon_r^{\text{inc}}(\vec{r})$) corresponds to the relative permeability (resp. permittivity) of the embedding medium. The incident field originates in the current distribution $\mathbf{J}(\vec{r})$.

In the presence of inhomogeneities, the field is perturbed and is now denoted as the total field, $\mathbf{E}^{\text{tot}}$, which satisfies a similar Helmholtz equation

$$\operatorname{div}\left(\frac{1}{\mu_r^{\text{tot}}}\operatorname{grad}\mathbf{E}^{\text{tot}}\right) + k_0^2\varepsilon_r^{\text{tot}}\mathbf{E}^{\text{tot}} = -jk_0Z_0\mathbf{J},\ \text{in}\ \Omega \tag{2}$$

where the relative permeability $\mu_r^{\text{tot}}(\vec{r})$ and permittivity $\varepsilon_r^{\text{tot}}(\vec{r})$ only differ from $\mu^{\text{inc}}(\vec{r})$ and $\varepsilon^{\text{inc}}(\vec{r})$ where the inhomogeneities are located.

From the linearity of Maxwell's equations, the total field can be decomposed into the incident field $\mathbf{E}^{\text{inc}}$ and a scattered field $\mathbf{E}^{\text{sc}}$ which also satisfies a Helmholtz equation

$$\operatorname{div}\left(\frac{1}{\mu_r^{\text{tot}}}\operatorname{grad}\mathbf{E}^{\text{sc}}\right) + k_0^2\varepsilon_r^{\text{tot}}\mathbf{E}^{\text{sc}} = \mathbf{J}^{\text{sc}}\ \text{in}\ \Omega \tag{3}$$

where the induced currents are defined as

$$\mathbf{J}^{\text{sc}} = -\operatorname{div}\left(\left[\frac{1}{\mu_r^{\text{tot}}} - \frac{1}{\mu_r^{\text{inc}}}\right]\operatorname{grad}\mathbf{E}^{\text{inc}}\right) - k_0^2\left[\varepsilon_r^{\text{tot}} - \varepsilon_r^{\text{inc}}\right]\mathbf{E}^{\text{inc}} \tag{4}$$

As the currents $\mathbf{J}$ and $\mathbf{J}^{\text{sc}}$ are referring to sources which are only located within the bounded domain Ω, we impose that the fields $\mathbf{E}^{\text{tot}}$, $\mathbf{E}^{\text{inc}}$ and $\mathbf{E}^{\text{sc}}$ satisfies a Sommerfeld radiation boundary condition on the external boundary $\partial\Omega$ of Ω. To ensure numerically that the computed fields satisfy this type of behavior, we have surrounded the external boundary of Ω with a cartesian Perfect Matched Layer (here a uni-axial media). Moreover, this type of material gives us the opportunity to test the proposed method against 2D anisotropic media.

3. FINITE ELEMENT TEARING AND INTERCONNECTING METHOD AND PROPOSED EXTENSION OF THE METHOD

This section is devoted to a thorough explanation of the proposed FETI method. Firstly, we explain how the various parameters (sub-domains, fields values, interface and corner nodes, ...) are defined. Secondly, as

our approach is an evolution of the FETI-DPEM2 method [27, 28], we recall the main idea of this method. We have deliberately followed the notations proposed in [27, 28]. Finally, we detail how we can extend this method in order to impose more flexible Robin-type boundary conditions everywhere, that is, on the edges related to the internal interfaces as well as the ones related to the corner points.

3.1. Geometrical Feature Extractions

We assume that the domain Ω is divided into a set of N_s non-overlapping domains:

$$\Omega = \bigcup_{i=1}^{N_s} \Omega^i, \quad \Omega^i \cap \Omega^j = \emptyset, \quad \forall i \neq j \tag{5}$$

where the index i denotes the subdomain number. For a given subdomain Ω^i, the indices of all its adjacent subdomains are called $neighbor(i)$. The internal boundary of the subdomain Ω^i is denoted as Γ^i. The internal boundary between two subdomains Ω^i and Ω^j, with $j \in neighbor(i)$, is denoted as Γ^{ij}.

In each subdomain, we are splitting the field unknowns in the following way:

$$E^i = \begin{bmatrix} E_V^i \\ E_I^i \\ \hline E_c^i \end{bmatrix} = \begin{bmatrix} E_r^i \\ E_c^i \end{bmatrix}, \tag{6}$$

where the notations E_r^i denote all the internal (V) and interface (I) points belonging to the i-th subdomain except for the corner points which are denoted by E_c^i. We now introduce several Boolean matrices to extract the node points of interest. The matrix $\mathbb{D}_r^i$ extracts from all the nodes of Ω^i the ones which are located on its interface, i.e.,

$$\mathbb{D}_r^i E_r^i = E_I^i \tag{7}$$

The matrices $\mathbb{T}_r^{i\to j}$ and $\mathbb{T}_c^{i\to j}$ extract the points of Ω^i which are also belonging to Ω^j, thus to Γ^{ij}. These matrices are defined such that

$$\mathbb{T}_r^{i\to j} E_I^i = E_r^{i\to j} \quad \text{and} \quad \mathbb{T}_c^{i\to j} E_c^i = E_c^{i\to j} \tag{8}$$

The same type of equation hold for the internal interface Γ^{ji} and for the subdomain Ω^j.

As continuity conditions must be enforced at each interface, we introduce a set of dual variables λ, which are also called Lagrange multipliers. It represents the contribution from the unknown mixed boundary condition at the edges related to the subdomain interfaces and the ones related to the corner points. As done in (6), we separate

the vector λ into its λ_r and λ_c parts. Two supplemental Boolean matrices $\mathbb{Q}^i_{\lambda_r}$ and $\mathbb{Q}^i_{\lambda_c}$ are introduced such that

$$\mathbb{Q}^i_{\lambda_r}\lambda_r = \lambda^i_r \quad \text{and} \quad \mathbb{Q}^i_{\lambda_c}\lambda_c = \lambda^i_c \tag{9}$$

where λ^i_r (resp. λ^i_c) are associated to the interface (resp. corner) points of the subdomain Ω^i. The set of Lagrange multipliers related to the internal interface Γ^{ij} are denoted as $\lambda^{i\to j}_r$ and $\lambda^{i\to j}_c$. Similarly as in (8) we can introduce two Boolean matrices to extract the unknown set of $\lambda^{i\to j}$ from the vector λ^i, i.e.,

$$\mathbb{T}^{i\to j}_{\lambda_r}\lambda^i_r = \lambda^{i\to j}_r \quad \text{and} \quad \mathbb{T}^{i\to j}_{\lambda_c}\lambda^i_c = \lambda^{i\to j}_c \tag{10}$$

The main specificity of the FETI-DPEM methods relies on the way the corner points are being handled. Indeed, in these methods, the main idea is to consider a single global numbering for the corner points. Thus, a global set of corner points $\mathbf{E}_c$ is defined. In order to facilitate the transition from the numbering in the global set of corner points to the numbering in the local set of corner points, we introduce a projection Boolean matrix $\mathbb{Q}^i_{\mathbf{E}_c}$ such that

$$\mathbb{Q}^i_c\mathbf{E}_c = E^i_c \tag{11}$$

With the help of the aforementioned extraction matrices, we can now rewrite the Helmholtz equation, taking into account the continuity conditions at the various interfaces.

3.2. FETI-DPEM2 Method

After having constructed an augmented Lagrangian functional and found its saddle-point thanks to the Karush-Kuhn-Tucker conditions [21, 24], we must solve the following equation, for each i-th subdomain,

$$K^iE^i = f^i - {\mathbb{D}^i}^T\lambda^i \tag{12}$$

where K^i is a sum of the stiffness matrix, the mass matrix and some elements related to the boundary conditions.

Following the idea of the FETI-DPEM2 method [27, 28], and the notations introduced in (6), we can rewrite (12) as follows

$$\begin{bmatrix} K^i_{rr} & K^i_{rc} \\ K^i_{cr} & K^i_{cc} \end{bmatrix} \begin{bmatrix} E^i_r \\ E^i_c \end{bmatrix} = \begin{bmatrix} f^i_r \\ f^i_c \end{bmatrix} - \begin{bmatrix} {\mathbb{D}^i_r}^T\lambda^i_r \\ \lambda^i_c \end{bmatrix} \tag{13}$$

From the first equation in (13), the electric field in the i-th subdomain can be found as

$$E^i_r = {K^i_{rr}}^{-1}(f^i_r - {\mathbb{D}^i_r}^T\lambda^i_r - K^i_{rc}E^i_c) \tag{14}$$

By eliminating E_r^i from the second line of (13), we obtain for E_c^i

$$\left(K_{cc}^i - K_{cr}^i {K_{rr}^i}^{-1} K_{rc}^i\right) E_c^i = f_c^i - \lambda_c^i - K_{cr}^i {K_{rr}^i}^{-1} f_r^i + K_{cr}^i {K_{rr}^i}^{-1} {\mathbb{D}_r^i}^T \lambda_r^i \quad (15)$$

By assembling all the subdomain contributions and summing them over i, the global corner points related system equation is obtained as follows

$$\mathrm{F}_{\mathbf{E}_c\mathbf{E}_c}\mathbf{E}_c - \mathrm{F}_{\mathbf{E}_c\lambda_r}\lambda_r - \mathrm{F}_{\mathbf{E}_c\lambda_c}\lambda_c = \mathrm{d}_{\mathbf{E}_c} \quad (16)$$

where

$$\begin{aligned}
\mathrm{F}_{\mathbf{E}_c\mathbf{E}_c} &= \sum_{i=1}^{N_s} \left[{\mathbb{Q}_c^i}^T K_{cc}^i \mathbb{Q}_c^i - \left(K_{rc}^i \mathbb{Q}_c^i\right)^T {K_{rr}^i}^{-1} \left(K_{rc}^i \mathbb{Q}_c^i\right)\right] \\
\mathrm{F}_{\mathbf{E}_c\lambda_r} &= \sum_{i=1}^{N_s} \left(\mathbb{D}_r^i {K_{rr}^i}^{-1} K_{rc}^i \mathbb{Q}_c^i\right)^T \mathbb{Q}_{\lambda_r}^i \\
\mathrm{F}_{\mathbf{E}_c\lambda_c} &= \sum_{i=1}^{N_s} {\mathbb{Q}_c^i}^T \mathbb{Q}_{\lambda_c}^i \\
\mathrm{d}_{\mathbf{E}_c} &= \sum_{i=1}^{N_s} \left({\mathbb{Q}_c^i}^T f_c^i - {\mathbb{Q}_c^i}^T {K_{rc}^i}^T {K_{rr}^i}^{-1} f_r^i\right)
\end{aligned}$$

We must now apply the boundary conditions between each subdomain. For each internal interface Γ^{ij}, we have

$$\lambda^{i\to j} + \lambda^{j\to i} = -\left(\mathrm{W}^{i\to j} + \mathrm{W}^{j\to i}\right) E^{j\to i} \quad \forall\, \Gamma^{ij} \quad (17)$$

where $W^{i\to j}$ enables to code quantities related to the projections of $E^{i\to j}$ on basis functions of Γ^{ij}. Following the notations introduced in (6), we can rewrite (17) as

$$\begin{bmatrix} \lambda_r^{i\to j} \\ \lambda_c^{i\to j} \end{bmatrix} + \begin{bmatrix} \lambda_r^{j\to i} \\ \lambda_c^{j\to i} \end{bmatrix} = -\begin{bmatrix} M_{rr}^{i\leftrightarrow j} & M_{rc}^{i\leftrightarrow j} \\ M_{cr}^{i\leftrightarrow j} & M_{cc}^{i\leftrightarrow j} \end{bmatrix} \begin{bmatrix} E_r^{j\to i} \\ E_c^{j\to i} \end{bmatrix} \quad \forall\, \Gamma^{ij} \quad (18)$$

where $M_{rr}^{i\leftrightarrow j} = W_{rr}^{i\to j} + W_{rr}^{j\to i}$.

In the FETI-DPEM2 method, described in [26, 27], the authors impose that

$$\begin{bmatrix} M_{rr}^{i\leftrightarrow j} & M_{rc}^{i\leftrightarrow j} \\ M_{cr}^{i\leftrightarrow j} & M_{cc}^{i\leftrightarrow j} \end{bmatrix} = \begin{bmatrix} M_{rr}^{i\leftrightarrow j} & 0 \\ 0 & 0 \end{bmatrix} \quad (19)$$

With this assumption in mind, let us focus on the first equation of (18), which is

$$\lambda_r^{i\to j} + \lambda_r^{j\to i} = -M_{rr}^{i\leftrightarrow j} E_r^{j\to i} \quad (20)$$

This expression is equivalent to applying a Robin-type boundary condition on the edges of the internal interfaces such as

$$\frac{1}{\mu_r^i}\frac{\partial E_r^i}{\partial n^i} + \alpha^i E_r^i = \Lambda^i \quad \text{and} \quad \frac{1}{\mu_r^j}\frac{\partial E_r^j}{\partial n^j} + \alpha^j E_r^j = \Lambda^j \quad \forall \Gamma^{ij} \tag{21}$$

We can eliminate $E_r^{j\to i}$ from (20) thanks to (14) and the Boolean matrices $\mathbb{T}_r^{j\to i}$ and $\mathbb{D}_r^i$. If we sum now (20) over j and afterwards over i, we obtain an equation linking λ_r and $\mathbf{E}_c$, which is

$$\mathrm{F}_{\lambda_r\lambda_r}\lambda_r - \mathrm{F}_{\lambda_r\mathbf{E}_c}\mathbf{E}_c = \mathrm{d}_{\lambda_r} \tag{22}$$

where

$$\mathrm{F}_{\lambda_r\lambda_r} = \mathbf{I} + \sum_{i=1}^{N_s} {\mathbb{Q}_{\lambda_r}^i}^T \sum_{j\in neighbor(i)} {\mathbb{T}_{\lambda_r}^{i\to j}}^T ({\mathbb{T}_{\lambda_r}^{j\to i}} - M_{rr}^{i\leftrightarrow j}{\mathbb{T}_{\lambda_r}^{j\to i}}F_{rr}^j)\mathbb{Q}_{\lambda_r}^j$$

$$\mathrm{F}_{\lambda_r\mathbf{E}_c} = \sum_{i=1}^{N_s} {\mathbb{Q}_{\lambda_r}^i}^T \sum_{j\in neighbor(i)} {\mathbb{T}_{\lambda_r}^{i\to j}}^T (M_{rr}^{i\leftrightarrow j}{\mathbb{T}_{\lambda_r}^{j\to i}}F_{rc}^j)$$

$$\mathrm{d}_{\lambda_r} = \sum_{i=1}^{N_s} {\mathbb{Q}_{\lambda_r}^i}^T \sum_{j\in neighbor(i)} {\mathbb{T}_{\lambda_r}^{i\to j}}^T M_{rr}^{i\leftrightarrow j}{\mathbb{T}_{\lambda_r}^{j\to i}}d_r^j$$

and

$$F_{rr}^i = \mathbb{D}_r^i {K_{rr}^i}^{-1} {\mathbb{D}_r^i}^T \tag{23}$$

$$F_{rc}^i = \mathbb{D}_r^i {K_{rr}^i}^{-1} K_{rc}^i \mathbb{Q}_c^i \tag{24}$$

$$d_r^i = \mathbb{D}_r^i {K_{rr}^i}^{-1} f_r^i \tag{25}$$

Let us now focus on the second row of (18), which is

$$\lambda_c^{i\to j} + \lambda_c^{j\to i} = 0 \quad \forall \Gamma^{ij} \tag{26}$$

Such relation between the Lagrange multipliers is equivalent to applying a Neumann-type boundary condition on the edges related to the corner points. It also implies that

$$\mathrm{F}_{\mathbf{E}_c\lambda_c}\lambda_c = \sum_{i=1}^{N_s} {\mathbb{Q}_c^i}^T \lambda_c^i = 0 \tag{27}$$

Finally, by combining (16) (22) and (27), we end up with the following set of equations

$$\begin{bmatrix} -\mathrm{F}_{\lambda_r\lambda_r} & \mathrm{F}_{\lambda_r\mathbf{E}_c} \\ \mathrm{F}_{\mathbf{E}_c\lambda_r} & -\mathrm{F}_{\mathbf{E}_c\mathbf{E}_c} \end{bmatrix} \begin{bmatrix} \lambda_r \\ \mathbf{E}_c \end{bmatrix} = - \begin{bmatrix} \mathrm{d}_{\lambda_r} \\ \mathrm{d}_{\mathbf{E}_c} \end{bmatrix} \tag{28}$$

Once λ_r and $\mathbf{E}_c$ are computed, the field can be estimated everywhere by applying (14).

3.3. Extension of the FETI-DPEM2 Method

In our approach, we propose to consider a Robin-type boundary condition for all edges on Γ^i, i.e., on the corner points as well. Thus, we will assume for now on that $M_{rc}^{i\leftrightarrow j} = M_{cr}^{i\leftrightarrow j} = M_{cc}^{i\leftrightarrow j} \neq 0$ in (18) or equivalently that (19) is no more valid. In that case, (28) is no more applicable and must be rewritten.

Let us focus on the first line of (18), which is now written with all the terms,

$$\lambda_r^{i\to j} + \lambda_r^{j\to i} = -M_{rr}^{i\leftrightarrow j} E_r^{j\to i} - M_{rc}^{i\leftrightarrow j} E_c^{j\to i} \tag{29}$$

As done previously, we can eliminate $E_r^{j\to i}$ from (29) thanks to (14) and the Boolean matrices $\mathbb{T}_r^{j\to i}$ and $\mathbb{D}_r^i$. We can also rewrite $E_c^{j\to i}$ as $\mathbb{T}_c^{j\to i}\mathbb{Q}_c^i\mathbf{E}_c$. We obtain an equation similar to (22), apart from $\mathrm{F}_{\lambda_r\mathbf{E}_c}$ which is replaced by

$$\tilde{\mathrm{F}}_{\lambda_r\mathbf{E}_c} = \sum_{i=1}^{N_s} {\mathbb{Q}_{\lambda_r}^i}^T \sum_{j\in neighbor(i)} {\mathbb{T}_{\lambda_r}^{i\to j}}^T (M_{rr}^{i\leftrightarrow j}\mathbb{T}_{\lambda_r}^{j\to i}F_{rc}^j - M_{rc}^{i\leftrightarrow j}\mathbb{T}_c^{j\to i}\mathbb{Q}_c^j)$$

Let us now focus on the second equation of (18), which corresponds now to

$$\lambda_c^{i\to j} + \lambda_c^{j\to i} = -M_{cr}^{i\leftrightarrow j} E_r^{j\to i} - M_{cc}^{i\leftrightarrow j} E_c^{j\to i} \tag{30}$$

This relation, unlike the FETI-DPEM2 method, applies the Robin-type boundary condition on the edges related to the corner points. By eliminating $E_r^{j\to i}$ and summing this equation over j and afterwards over i, we obtain a new equation linking λ_r, λ_c and $\mathbf{E}_c$

$$-\tilde{\mathrm{F}}_{\lambda_c\lambda_r}\lambda_r + \tilde{\mathrm{F}}_{\lambda_c\mathbf{E}_c}\mathbf{E}_c + \tilde{\mathrm{F}}_{\lambda_c\lambda_c}\lambda_c = \tilde{\mathrm{d}}_{\lambda_c} \tag{31}$$

where

$$\tilde{\mathrm{F}}_{\lambda_c\lambda_r} = \sum_{i=1}^{N_s} {\mathbb{Q}_{\lambda_c}^i}^T \sum_{j\in neighbor(i)} {\mathbb{T}_{\lambda_c}^{i\to j}}^T \left(M_{cr}^{i\leftrightarrow j}\mathbb{T}_r^{j\to i}F_{rr}^j\right)\mathbb{Q}_{\lambda_r}^j$$

$$\tilde{\mathrm{F}}_{\lambda_c\mathbf{E}_c} = \sum_{i=1}^{N_s} {\mathbb{Q}_{\lambda_c}^i}^T \sum_{j\in neighbor(i)} {\mathbb{T}_{\lambda_c}^{i\to j}}^T \left(M_{cr}^{i\leftrightarrow j}\mathbb{T}_r^{j\to i}F_{rc}^j - M_{cc}^{i\leftrightarrow j}\mathbb{T}_c^{j\to i}\mathbb{Q}_c^j\right)$$

$$\tilde{\mathrm{F}}_{\lambda_c\lambda_c} = \mathbf{I} + \sum_{i=1}^{N_s} {\mathbb{Q}_{\lambda_c}^i}^T \sum_{j\in neighbor(\Omega^i)} {\mathbb{T}_{\lambda_c}^{i\to j}}^T \mathbb{T}_{\lambda_c}^{j\to i}\mathbb{Q}_{\lambda_c}^j$$

$$\tilde{\mathrm{d}}_{\lambda_c} = \sum_{i=1}^{N_s} {\mathbb{Q}_{\lambda_c}^i}^T \sum_{j\in neighbor(i)} {\mathbb{T}_{\lambda_c}^{i\to j}}^T \left(M_{cr}^{i\leftrightarrow j}\mathbb{T}_r^{j\to i}d_r^j\right)$$

It also implies that, in our proposed approach,

$$\mathrm{F}_{\mathbf{E}_c\lambda_c}\lambda_c = \sum_{i=1}^{N_s} \mathbb{Q}_c^{i\,T}\lambda_c^i \neq 0$$

Combining (16), the modified (22) and (31) leads us to a completely new system

$$\begin{bmatrix} -\mathrm{F}_{\lambda_r\lambda_r} & \tilde{\mathrm{F}}_{\lambda_r\mathbf{E}_c} & 0 \\ \mathrm{F}_{\mathbf{E}_c\lambda_r} & -\mathrm{F}_{\mathbf{E}_c\mathbf{E}_c} & \mathrm{F}_{\mathbf{E}_c\lambda_c} \\ \tilde{\mathrm{F}}_{\lambda_c\lambda_r} & -\tilde{\mathrm{F}}_{\lambda_c\mathbf{E}_c} & -\tilde{\mathrm{F}}_{\lambda_c\lambda_c} \end{bmatrix} \begin{bmatrix} \lambda_r \\ \mathbf{E}_c \\ \lambda_c \end{bmatrix} = - \begin{bmatrix} \mathrm{d}_{\lambda_r} \\ \mathrm{d}_{\mathbf{E}_c} \\ \tilde{\mathrm{d}}_{\lambda_c} \end{bmatrix} \tag{32}$$

The introduction of the new unknown λ_c in this system is computationally reasonable as there are in fact very few corner points whatever the selected partition. Nevertheless, as shown in the next session, this parameter has great influence on the accuracy of the computed fields.

4. NUMERICAL RESULTS

In this section, we compare the field computed thanks to the various approaches in the framework of a 2D scattering configuration. We assume that the domain Ω is filled with air. The operating frequency is 800 MHz. The domain is a square whose size is $[8 \times 8]\,\mathrm{m}^2 \approx 21 \times 21\lambda$. One line source, located at (2.5, 2.5) m radiates a s-polarized wave. Three square scatterers are positioned inside the domain Ω. All the scatterers are assumed to be non-magnetic ($\mu_r = 1$), and they present a relative permittivity respectively equal to $\varepsilon_r^1 = 1.5$, $\varepsilon_r^2 = 3.0$, and $\varepsilon_r^3 = 5.0$. The domain is surrounded by a cartesian uni-axial Perfectly Matched Layer (PML) whose width is 1 m (Figure 1). It must be noticed here that we have used the scattered field formulation even if the source is enclosed in the computational domain.

The domain is discretized thanks to a free unstructured mesh generator GMSH [37]. The global mesh contains 214 429 nodes and 430 510 triangles. This global mesh is inserted into a home-made mesh partitioner which provides, for each subdomain, the structure of the local mesh as well as the boundaries and the corner nodes lists between subdomains. This partitioner intensively uses subroutines provided by METIS [38]. The factorization of each sub-matrices is performed thanks to a direct sparse solver [9, 10] and stored during the resolution of the interface problem. The interface problem uses a crude GMRES method without any preconditioner.

The scattered field $\mathbf{E}^{\mathrm{sc}}$ is computed using three different approaches. In the first one, denoted in the following as FEM, the

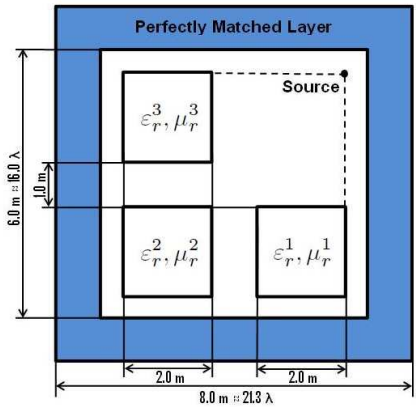

Figure 1. Position of the source in the area filled with air and bounded with PML with the 3 scatterers inside.

field $\mathbf{E}_1^{\text{sc}}$ is computed by solving (3) taking into account the whole domain, without any partitioning. In the second one, denoted simply as FETI-DPEM2, the domain is partitioned and the system defined in (28) is solved to provide $\mathbf{E}_{N_s}^{\text{sc}}$. In the last one, denoted as FETI-DPEM2 extended, the partitioning is again employed but this time the extended system defined in (32) is solved, taking into account the Lagrange multipliers for the corner points, to provide $\mathbf{E}_{N_s,ext}^{\text{sc}}$. We have defined a L^2-norm error between the various scattered fields,

$$L_{N_s}^2 = \frac{\| \mathbf{E}_{N_s}^{\text{sc}} - \mathbf{E}_1^{\text{sc}} \|^2}{\| \mathbf{E}_1^{\text{sc}} \|^2} \quad \text{and} \quad L_{N_s,ext}^2 = \frac{\| \mathbf{E}_{N_s,ext}^{\text{sc}} - \mathbf{E}_1^{\text{sc}} \|^2}{\| \mathbf{E}_1^{\text{sc}} \|^2}$$

For a domain divided into 5 subdomains ($N_s = 5$), the scattered field is presented in Figure 2. The L^2-norm error between the various computed fields is such that $L_{N_s}^2 = 4.00\,10^{-3}$ and $L_{N_s,ext}^2 = 7.88\,10^{-13}$. As this error might evolve with N_s, we have solved the same scattering problem for different number of partitions (see Table 1). Two main features can be deduced from Table 1. Firstly, our proposed method is very stable against the number of subdomains. Secondly, the L^2-norm error is always smaller for the extended FETI-DPEM2 approach than for the classical FETI-DPEM2 approach.

This is probably due to the fact that the final values obtained at each corner points of the domain with the FETI-DPEM2 extended method have a better agreement than the ones obtained with classical FETI-DPEM2 method. This is confirmed by the results shown in Figure 3 in which we have plotted the values of the electric field obtained by the three methods when the domain Ω is divided into

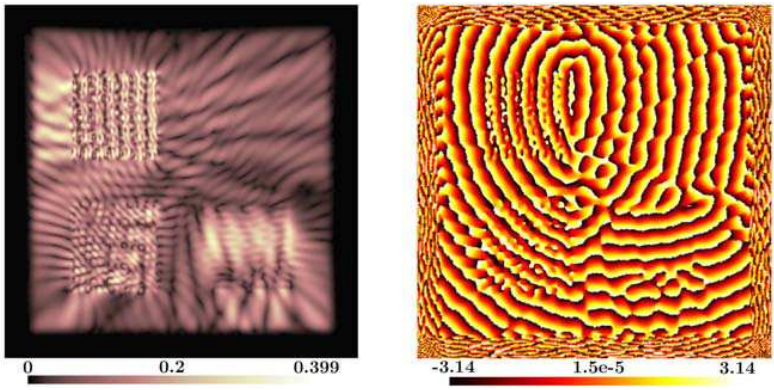

Figure 2. Map of the scattered field when three scatterers (with $\varepsilon_r^1 = 1.5$, $\varepsilon_r^2 = 3.0$, $\varepsilon_r^3 = 5.0$) are illuminated by a line source (see Figure 1). A partitioning in $N_s = 5$ subdomains is used. (a) Amplitude (lin.). (b) Phase (rad).

Table 1. Relative L^2-norm errors when different methods and different partitioning are used.

N_s	FETI-DPEM2 ($L^2_{N_s}$)	FETI-DPEM2 extended ($L^2_{N_s,ext}$)
5	$4.00\,10^{-3}$	$7.88\,10^{-13}$
10	$2.05\,10^{-2}$	$6.81\,10^{-12}$
15	$3.93\,10^{-2}$	$6.97\,10^{-12}$
20	$5.04\,10^{-2}$	$2.58\,10^{-11}$
25	$7.43\,10^{-2}$	$5.07\,10^{-11}$
30	$8.23\,10^{-2}$	$2.45\,10^{-11}$

17 partitions yielding 22 corner points. The partitioned geometry is represented in Figure 4.

Figure 4 is also pointing out the fact that the domain is partitioned in a non-regular manner. The interfaces Γ^{ij} are definitely not straight lines and this might influence the way the transmission boundary conditions are being applied between each subdomain. Nevertheless, Table 1 guaranties that numerically, even when N_s increases, the interface boundary conditions are correctly taken into account. An other key-parameter in the Robin-type boundary conditions is the coefficient α^i (see (21)). We have thus tested the convergence of the method with respect to α^i. For the same value of the stopping criterion of the GMRES algorithm, we have noted in Table 2 the value chosen for α^i, the number of iterations of the GMRES algorithm as well as

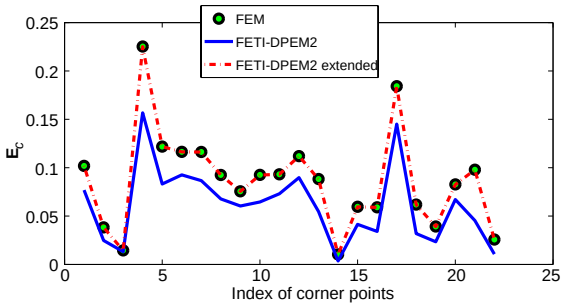

Figure 3. Amplitude of the electrical field $\mathbf{E}^{\text{sc}}$ extracted at the corner points when different methods are employed. The partition with $N_s = 17$ is shown in Figure 4.

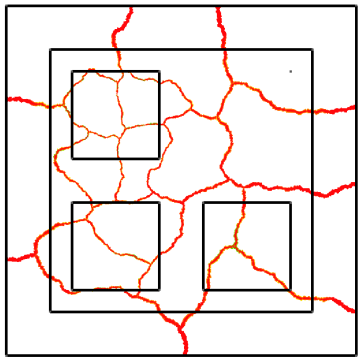

Figure 4. Map of the schematic domain, showing the way the partitioning has been performed for $N_s = 17$.

Table 2. Number of iterations and relative error of the FETI-DPEM2 extended method when different values of α^i are used.

$\alpha^i/(jk_0)$	Number of iterations	Relative error $(L^2_{N_s,ext})$
1.0	1 181	$1.96\,10^{-11}$
2.0	1 611	$4.49\,10^{-11}$
average	1 091	$8.58\,10^{-12}$

the L^2-norm error obtained with the FETI-DPEM2 extended method.

The value noted as *average* corresponds to $\frac{\alpha^i}{jk_0} = \frac{\sqrt{\mu_r^i\varepsilon_r^i}+\sqrt{\mu_r^k\varepsilon_r^k}}{2}$ which is the value suggested in [33]. As one can remark, this value is also an optimal value in terms of iterations for our proposed method. Furthermore, this value provides a very stable and precise solution of the considered problem even with anisotropic medias.

5. CONCLUSION

In this paper, we have presented the simulation results obtained using a modified approach of the FETI-DPEM2 method. Indeed, a new set of Lagrange multipliers have been added in order to handle the continuity conditions differently at the corner points between the various subdomains. The numerical results presented here have shown that the introduction of this new set enables to provide more accurate results with respect to the classical FETI-DPEM2 method. Moreover, we have been able to partite and handle internal interfaces which are not necessarily straight lines without major drawback in terms of computational accuracy. One possible path of investigation is to implement not only first-order transmission boundary conditions but also second-order transmission boundary conditions at the edges related to the internal interfaces as well as the ones related to the corner points and to analyze their influences in terms of algorithm complexity and computational efficiency.

The problem of interest that we analyzed here is based on a scattered field formulation. We have investigated so far a two-dimensional configuration and are currently working on the three-dimensional extension of this problem. There are no restriction for taking into account scatterers which are made of heterogeneous structures or even anisotropic materials.

REFERENCES

1. Peterson, A. F., S. L. Ray, and R. Mittra, *Computational Methods for Electromagnetics,* Oxford University Press, 1998.
2. Jin, J., *The Finite Element Method in Electromagnetics,* John Wiley & Sons, 2002.
3. Volakis, J. L., A. Chatterjee, and L. C. Kempel, *Finite Element Method for Electromagnetics with Application to Antennas, Microwave Circuits, and Scattering,* IEEE Press, 1998.
4. Otin, R., L. E. Garcia-Castillo, I. Martinez-Fernandez, and D. Garcia-Donoro, "Computational performance of a weighted regularized Maxwell equation finite element formulation," *Progress In Electromagnetics Research*, Vol. 136, 61–77, 2013.
5. Dziekonski, A., P. Sypek, A. Lamecki, and M. Mrozowski, "Finite element matrix generation on a GPU," *Progress In Electromagnetics Research*, Vol. 128, 249–265, 2012.
6. Gomez-Revuelto, I., L. E. Garcia-Castillo, and L. F. Demkowicz, "A comparison between PML, infinite elements and an iterative

BEM as mesh truncation methods for HP self-adaptive procedures in electromagnetics," *Progress In Electromagnetics Research*, Vol. 126, 499–519, 2012.

7. Gomez-Revuelto, I., L. E. Garcia-Castillo, and M. Salazar-Palma, "Goal-oriented self-adaptive HP-strategies for finite element analysis of electromagnetic scattering and radiation problems," *Progress In Electromagnetics Research*, Vol. 125, 459–482, 2012.
8. Otin, R. and H. Gromat, "Specific absorption rate computations with a nodal-based finite element formulation," *Progress In Electromagnetics Research*, Vol. 128, 399–418, 2012.
9. Amestoy, P. R., I. S. Du, and J.-Y. L'Excellent, "Multifrontal parallel distributed symmetric and unsymmetric solvers," *Comput. Methods in Appl. Mech. Eng.*, Vol. 184, 501–520, 2000, See Internet Address: http://graal.ens-lyon.fr/MUMPS.
10. Amestoy, P. R., I. S. Du, J. Koster, and J.-Y. L'Excellent, "A fully asynchronous multifrontal solver using distributed dynamic scheduling," *SIAM Journal on Matrix Analysis and Applications*, Vol. 23, No. 1, 15–41, 2001.
11. "WSMP: Watson sparse matrix package," See Internet Address: http://www-users.cs.umn.edu/∼agupta/wsmp.html.
12. Davis, T. A., "Algorithm 832: UMFPACK, an unsymmetricpattern multifrontal method," *ACM Transactions on Mathematical Software*, Vol. 30, No. 2, 196–199, 2004.
13. Zhu, Y. and A. C. Cangellaris, *Multigrid Finite Element Method for Electromagnetic Field Modeling,* Wiley-IEEE Press, 2006.
14. Ernst, O. G. and M. J. Gander, "Why is it dicult to solve Helmholtz problems with classical iterative methods," *Numerical Analysis of Multiscale Problems*, Vol. 83, 325–361, 2011.
15. Zhao, K., M. N. Vouvakis, and J.-F. Lee, "Application of DPFETI domain decomposition method for the negative index of refraction materials," *IEEE Antennas and Propagation Society International Symposium*, Vol. 3B, 26–29, 2005.
16. Zhao, K. and J.-F. Lee, "An accelerated non-conforming DP-FETI domain decomposition method for the analysis of large EMC problems," *Electromagnetic Compatibility Symposium*, 200–203, 2006.
17. Zhao, K., V. Rawat, S.-C. Lee, and J.-F. Lee, "A domain decomposition method with nonconformal meshes for nite periodic and semi-periodic structures," *IEEE Transactions on Antennas and Propagation*, Vol. 55, No. 9, 2559–2570, 2007.
18. Zhao, K., V. Rawat, and J.-F. Lee, "A domain decomposition method for electromagnetic radiation and scattering analysis of

multi-target problems," *IEEE Transactions on Antennas and Propagation*, Vol. 56, No. 8, 2211–2221, 2008.

19. Farhat, C. and J. Mandel, "The two-level FETI method for static and dynamic plate problems — Part I: An optimal iterative solver for biharmonic systems," *Computer Methods in Applied Mechanics and Engineering*, Vol. 155, Nos. 1–2, 129–151, 1998.
20. Farhat, C., P. S. Chen, J. Mandel, and F. X. Roux, "The two-level FETI method — Part II: Extension to shell problems, parallel implementation and performance results," *Computer Methods in Applied Mechanics and Engineering*, Vol. 155, Nos. 1–2, 153–179, 1998.
21. Farhat, C., A. Macedo, M. Lesoinne, F. X. Roux, F. Magoules, and A. de la Bourdonnaie, "Two-level domain decomposition methods with Lagrange multipliers for the fast iterative solution of acoustic scattering problems," *Computer Methods in Applied Mechanics and Engineering*, Vol. 184, Nos. 2–4, 213–239, 2000.
22. Farhat, C., P. Avery, R. Tezaur, and J. Li, "FETI-DPH: A dual-primal domain decomposition method for acoustic scattering," *Journal of Computational Acoustics*, Vol. 13, No. 3, 499–524, 2005.
23. Boubendir, Y., X. Antoine, and C. Geuzaine, "A quasi-optimal non-overlapping domain decomposition algorithm for the Helmholtz equation," *Journal of Computational Physics*, Vol. 231, No. 2, 262–280, 2012.
24. Farhat, C., A. Macedo, and M. Lesoinne, "A two-level domain decomposition method for the iterative solution of high frequency exterior Helmholtz problems," *Numerische Mathematik*, Vol. 85, No. 2, 283–308, 2000.
25. Farhat, C., R. Tezaur, and J. Toivanen, "A domain decomposition method for discontinuous Galerkin discretizations of Helmholtz problems with plane waves and Lagrange multipliers," *International Journal For Numerical Methods in Engineering*, Vol. 78, No. 13, 1513–1531, 2009.
26. Li, Y. and J.-M. Jin, "A vector dual-primal nite element tearing and interconnecting method for solving 3-D large-scale electromagnetic problems," *IEEE Transactions on Antennas and Propagation*, Vol. 54, No. 10, 3000–3009, 2006.
27. Li, Y.-J. and J.-M. Jin, "A new dual-primal domain decomposition approach for nite element simulation of 3-D large-scale electromagnetic problems," *IEEE Transactions on Antennas and Propagation*, Vol. 55, No. 10, 2803–2810, 2007.
28. Li, Y.-J. and J.-M. Jin, "Implementation of the second-order ABC in the FETI-DPEM method for 3D EM problems," *IEEE*

Transactions on Antennas and Propagation, Vol. 56, No. 8, 2765–2769, 2008.

29. Dolean, V., S. Lanteri, and R. Perrussel, "A domain decomposition method for solving the three-dimensional time-harmonic Maxwell equations discretized by discontinuous Galerkin methods," *Journal of Computational Physics*, Vol. 227, No. 3, 2044–2072, 2008.
30. Dolean, V., M. J. Gander, and L. Gerardo-Giorda, "Optimized Schwarz methods for Maxwell's equations," *SIAM Journal on Scientic Computing*, Vol. 31, No. 3, 2193–2213, 2009.
31. Dolean, V., M. El Bouajaji, M. J. Gander, and S. Lanteri, "Optimized Schwarz methods for Maxwell's equations with nonzero electric conductivity," *Domain Decomposition Methods in Science and Engineering XIX*, Vol. 78, 269–276, 2011.
32. Fernandez-Recio, R., L. E. Garcia-Castillo, S. Llorente-Romano, and I. Gomez-Revuelto, "Convergence study of a non-standard Schwarz domain decomposition method for finite element mesh truncation in electro-magnetics," *Progress In Electromagnetics Research*, Vol. 120, 439–457, 2011.
33. Vouvakis, M. N., Z. Cendes, and J.-F. Lee, "A FEM domain decomposition method for photonic and electromagnetic band gap structures," *IEEE Transactions on Antennas and Propagation*, Vol. 54, No. 2, 721–733, 2006.
34. Xue, M.-F. and J.-M. Jin, "Nonconformal FETI-DP methods for large-scale electromagnetic simulation," *IEEE Transactions on Antennas and Propagation*, Vol. 60, No. 9, 4291–4305, 2012.
35. Dolean, V., S. Lanteri, and R. Perrussel, "Optimized Schwarz algorithms for solving time-harmonic Maxwell's equations discretized by a discontinuous Galerkin method," *IEEE Transactions on Magnetics*, Vol. 44, No. 6, 954–957, 2008.
36. Farhat, C., M. Lesoinne, P. LeTallec, K. Pierson, and D. Rixen, "FETI-DP: A dual-primal unied FETI method — Part I: A faster alternative to the two-level FETI method," *International Journal for Numerical Methods in Engineering*, Vol. 50, No. 7, 1523–1544, 2001.
37. Geuzaine, C. and J. F. Remacle, "GMSH: A three-dimensional finite element mesh generator with built-in pre- and post-processing facilities," See Internet Address: http://www.geuz.org/gmsh/.
38. Karipis, "METIS — Family of multilevel partitioning algorithms," See Internet Address: http://glaros.dtc.umn.edu/gkhome/views/metis.